Efficacy of the DFT + U formalism for modeling hole polarons in perovskite oxides

Paul Erhart,[1,*] Andreas Klein,[2] Daniel Åberg,[3] and Babak Sadigh[3]

[1]*Chalmers University of Technology, Department of Applied Physics, S-412 96 Gothenburg, Sweden*

[2]*Technische Universität Darmstadt, Institut für Materialwissenschaft, 64287 Darmstadt, Germany*

[3]*Lawrence Livermore National Laboratory, Chemistry, Materials and Life Sciences Directorate, Livermore, California 94550, USA*

(Received 3 February 2014; revised manuscript received 22 May 2014; published 17 July 2014)

We investigate the formation of self-trapped holes (STH) in three prototypical perovskites ($SrTiO_3$, $BaTiO_3$, $PbTiO_3$) using a combination of density functional theory (DFT) calculations with local potentials and hybrid functionals. First we construct a local correction potential for polaronic configurations in $SrTiO_3$ that is applied via the DFT + U method and matches the forces from hybrid calculations. We then use the DFT + U potential to search the configuration space and locate the lowest energy STH configuration. It is demonstrated that both the DFT + U potential and the hybrid functional yield a piecewise linear dependence of the total energy on the occupation of the STH level, suggesting that self-interaction effects have been properly removed. The DFT + U model is found to be transferable to $BaTiO_3$ and $PbTiO_3$, and STH formation energies from DFT + U and hybrid calculations are in close agreement for all three materials. STH formation is found to be energetically favorable in $SrTiO_3$ and $BaTiO_3$ but not in $PbTiO_3$, which can be rationalized by considering the alignment of the valence band edges on an absolute energy scale. In the case of $PbTiO_3$ the strong coupling between Pb 6s and O 2p states lifts the valence band minimum (VBM) compared to $SrTiO_3$ and $BaTiO_3$. This reduces the separation between VBM and STH level and renders the STH configuration metastable with respect to delocalization (band hole state). We expect that the present approach can be adapted to study STH formation also in oxides with different crystal structures and chemical compositions.

DOI: 10.1103/PhysRevB.90.035204 PACS number(s): 71.38.Ht, 77.84.Bw, 71.15.Mb, 77.84.Cg

I. INTRODUCTION

In materials with at least partially ionic bonding character, most notably halides and oxides, charge excitations can couple to lattice modes, leading to the formation of polarons [1–3]. In the limit where the coupling between charge excitations and phonons is strong, one obtains so-called small or Holstein polarons [4], which are characterized by very large but localized lattice distortions. Their motion can be considered classical [2,5] and typically exhibits an exponential temperature dependence. As a result the presence of polarons usually implies low mobilities, which are detrimental for many applications.

Perovskite oxides exhibit a broad variety of interesting phenomena including but not limited to ferroelectricity, multiferroicity, strong correlation, and low-dimensional electron gases. Applications are abundant as well as they are being used for example in electronics, catalysis, and thermoelectrics. Polaronic effects in these materials have been discussed for some time [1,6–8] and have also been investigated theoretically [9–13]. While the existence of "bound" small hole polarons,[1] which are associated for example with acceptor defects in oxides, is well established and rather common, the presence of "free" (or self-trapped) polarons in oxides, which are naturally also much harder to observe, has been doubted [1]. By contrast, earlier computational studies did identify hole polarons in $BaTiO_3$ based on embedded cluster Hartree-Fock (HF) calculations [9,10] and $SrTiO_3$ based on a suitably parametrized many-body model Hamiltonian [11,12] while electron polarons were studied for example in $KNbO_3$ and $KTaO_3$ [14]. This provides the motivation for the present work, in which we explore self-trapped hole (STH) polarons in three prototypical perovskite oxides, $SrTiO_3$, $BaTiO_3$, and $PbTiO_3$. As discussed in detail below, the description of polaronic effects is sensitive to the level of theory that is being employed. We therefore compare different techniques and carefully assess their respective predictiveness. We find that self-trapped polarons are energetically favorable in both $SrTiO_3$ and $BaTiO_3$ but not in $PbTiO_3$. The formation energies for small polarons in the first two materials are -0.1 eV and -0.2 eV, respectively, whereas the associated lattice distortions are less than 0.12 Å for individual atoms. The lack of spontaneous STH formation in $PbTiO_3$ can be traced to the strong coupling between Pb 6s and O 2p states, which raises the valence band maximum. The observed correlation between STH formation energies and VBM position suggests a simple approximate predictor for STH formation in this class of materials.

In the following section we discuss shortcomings of common electronic structure methods such as density functional theory (DFT) and HF as well as related approaches with respect to the description of polarons. In particular we argue for the suitability of the DFT + U method [15] for describing the systems of interest in this work. In Sec. III A it is shown that DFT + U functionals can be parametrized to reproduce the forces obtained from higher level (and computationally much more expensive) calculations based on hybrid exchange-correlation (XC) functionals. Using a suitable parametrization we then explore in Sec. III B the STH configuration space in the case of $SrTiO_3$, identify as well as characterize the ground-state configuration, and verify the results by comparison with hybrid XC functional calculations. In Sec. III C we then demonstrate that both DFT + U and hybrid XC calculations yield piecewise

*erhart@chalmers.se

[1]In particular in the titanates one can also observe electron polarons, which are associated with the reduction of Ti^{4+} to Ti^{3+}.

linear behavior for the total energy as a function of fractional charge, which demonstrates their suitability for the present purpose and supports their predictiveness. Finally, Sec. III E presents results for $BaTiO_3$ and $PbTiO_3$, which are rationalized in terms of the valence band alignment between the different materials.

II. METHODOLOGY

Density functional theory (DFT) based on semilocal XC functionals is a powerful tool for electronic structure calculations. It fails, however, to reproduce polaron formation in many condensed systems not only quantitatively but qualitatively [16,17]. This shortcoming can be traced to the self-interaction (SI) intrinsic to common semilocal approximations to the XC functional including the local density approximation (LDA) as well as the generalized gradient approximation (GGA). The importance of SI corrections in calculations based on semilocal XC functionals was first discussed by Perdew and Zunger [18], who also proposed a correction scheme that works well for atoms but falls short when it comes to molecules or solids. The issue has been addressed more recently in terms of variation of the total energy with respect to fractional changes in the electronic occupations [19–22]. An exact functional should lead to piecewise linear behavior with discontinuous derivatives at integer occupations [20]. DFT calculations based on semilocal XC functionals deviate from this requirement and overbind (concave dependence), whereas HF calculations tend to underbind (convex dependence) [23,24]. These opposite behaviors can be exploited in parametrizations of hybrid functionals that minimize the deviation from piecewise linearity [21].

The overbinding of LDA or GGA and associated lack of localization is also at the heart of another DFT failure that is associated with partially occupied d states in transition metal oxides, which are erroneously predicted to be metallic. The DFT + U (originally LDA + U) method [15], which was proposed to overcome this error, adds a Hubbard-like term to the total energy functional and solves it using the self-consistent field approach in the independent particle approximation. Hence, the standard DFT+U approach treats the Hubbard term within the mean-field approximation. Consequently, this method effectively adds a Fock-exchange term inside each atomic sphere to the standard LDA or GGA functionals:

$$E_{\mathrm{DFT}+U} = E_{\mathrm{DFT}} + \frac{1}{2}\sum_{I\alpha} U_\alpha n_{I,\alpha}(1 - n_{I,\alpha}). \qquad (1)$$

Above the summation runs over sites I and projection channels α, and $n_{I\alpha}$ is the occupancy of chancel α at site I. The resulting correction is quadratic in the occupancies and it was argued that self-consistent U parameters [25] should correspond to piecewise linear behavior [19]. The DFT + U approach was originally derived to account for the extra on-site Coulomb repulsion that occurs in strongly correlated systems due to the coexistence of atomiclike d or f electron states with delocalized band states. However, considering the mathematical similarity of the DFT + U method to hybrid DFT techniques, it should in principle also be appropriate for treating atomiclike polaronic states in normal insulators, which often possess p character, no matter whether they happen to be bound to point defects such as vacancies or have been self-trapped by lattice distortions. The hole states derived from O $2p$ orbitals in wide band-gap oxides constitute a large class of problems that fall into this category.

In order to establish a more detailed understanding of the applicability of the DFT + U method to the problem of polarons in insulators, we discuss here polarons in two classes of wide band-gap insulators: halides and functional oxides. In halides the formation of an STH[2] occurs by dimerization of two halogen ions, which can be formally described as the reaction $X^- + X^- + h^\bullet \rightarrow X_2^-$, where X represents the halogen and $h^\bullet$ denotes the band hole that is trapped in the process. The trapped hole is localized *between* the two halogens. By contrast, in oxides hole self-trapping is a single-center process [1] corresponding to the reduction of an oxygen ion $O^{2-} + h^\bullet \rightarrow O^-$. Let us now consider a charge balanced oxide crystal comprising N oxygen atoms, from which one electron is removed. STH formation implies $NO^{2-} + h^\bullet \rightarrow (N-1)O^{2-} + O^-$ whereas LDA or GGA yield $NO^{2-} + h^\bullet \rightarrow NO^{2-+1/N}$. This is related to the lack of charge disproportionation in partially filled d states for, e.g., ions in solution [27] and similarly originates from the overbinding or lack of localization in LDA-GGA alluded to above. This motivates the addition of a DFT + U term to the total energy functional where the penalty term is applied to the O $2p$ states. This approach is similar to the potential operator defined in Ref. [21].

In the present work we employ hybrid functionals as well as the DFT + U method, and check their predictions with regard to piecewise linearity. It should be pointed out that hybrid functionals are more generally applicable but at the same time computationally much more expensive than DFT + U calculations. All calculations were carried out using the projector augmented wave method [28] as implemented in the Vienna *ab initio* simulation package [29] using a plane-wave energy cutoff of 500 eV for volume relaxations and 400 eV otherwise. We used the LDA functional in combination with the DFT + U method in its simplified (rotationally invariant) form [15,30]. Hybrid DFT calculations were performed using the range-separated HSE06 functional [31,32].

III. RESULTS

A. LDA + U model for sampling the energy landscape

Let us first consider STH formation in the cubic phase of $SrTiO_3$and determine the associated lattice distortion. While an *a priori* assumption regarding the geometric structure or symmetry of the ionic displacements belong to the STH should be avoided, an exhaustive search over configurations using a hybrid functional is computationally exceedingly prohibitive. LDA or GGA calculations on the other hand fail to produce STH formation altogether, which is not surprising based on previous experience with STH formation in halides [16]. In fact, the forces computed within the LDA differ substantially from those obtained from HSE06 calculations, as evident from

[2]In halides STH configurations are for historical reasons commonly referred to as V_K centers, Ref. [26].

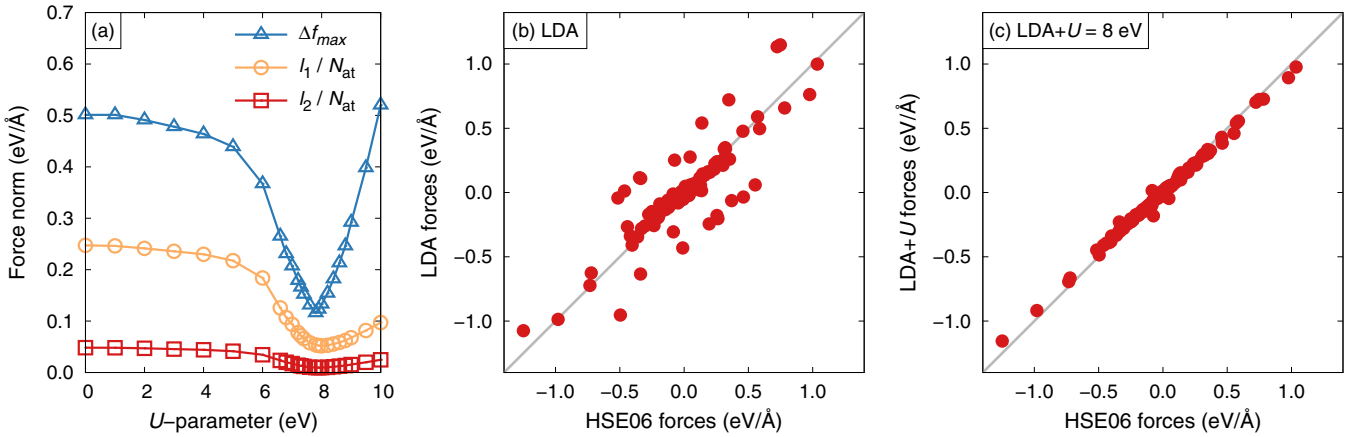

FIG. 1. (Color online) (a) Force matching between LDA + U models with U applied to O $2p$ states and the HSE06 hybrid functional for cubic $SrTiO_3$ based on l_1 and l_2 norm as well as maximum deviation of forces Δf_{max} (40-atom cell, one hole). Comparison of force components from (b) LDA ($U = 0$ eV) and (c) LDA + U with $U = 8$ eV with HSE06 calculations.

the leftmost data points in Fig. 1(a) as well as Fig. 1(b). These forces were computed for a $2 \times 2 \times 2$ $SrTiO_3$ supercell with one electron removed from the system and random displacements drawn from a Gaussian distribution with a standard deviation of 0.02 Å using a $2 \times 2 \times 2$ Monkhorst-Pack mesh for sampling the Brillouin zone.

Based on the arguments provided in the previous section there could, however, exist a DFT + U parametrization that yields an energy landscape in closer agreement with the HSE06 data. This is indeed the case as illustrated in Fig. 1(a), which shows the maximum difference between equivalent atomic forces from HSE06 and LDA + U calculations, $\Delta f_{\max} = \max_i\{|\boldsymbol{f}_i^{\mathrm{LDA}+U} - \boldsymbol{f}_i^{\mathrm{HSE06}}|\}$, along with the l_1 and l_2 norms of the force difference vector, which are defined as

$$l_1 = N^{-1} \sum_i^N \left| \boldsymbol{f}_i^{\mathrm{LDA}+U} - \boldsymbol{f}_i^{\mathrm{HSE06}} \right|, \tag{2}$$

$$l_2 = N^{-1} \sum_i^N \left(\boldsymbol{f}_i^{\mathrm{LDA}+U} - \boldsymbol{f}_i^{\mathrm{HSE06}} \right)^2, \tag{3}$$

where N is the number of atoms. Note that the LDA + U potential is applied to the O $2p$ state. Very close agreement is obtained for $U \approx 8$ eV as further illustrated by direct comparison of all force components in Fig. 1(c). We also considered random displacements with larger amplitudes corresponding to standard deviations of 0.05 and 0.10 Å, which resulted in maximum forces in excess of 3 and 11 eV/Å, respectively, and observed similarly good agreement.

B. Geometric and electronic structures of STH in $SrTiO_3$

The LDA + U calculations for the systems of interest in this work are more than two orders of magnitude faster than equivalent hybrid calculations and therefore enabled us to carry out a systematic search for minima in the potential energy landscape. To this end, configurations based on $3 \times 3 \times 3$ supercells were created by randomizing the atomic positions with displacement amplitudes up to 0.5 Å and using different random number seeds. Additional configurations were set up to explore the possibility of O–O dimerization along different crystallographic directions. The initial configurations were relaxed using conjugate gradient minimization and a $2 \times 2 \times 2$ Monkhorst-Pack mesh until the maximum force fell below 20 meV/Å.[3] In addition molecular dynamics simulations were carried out using $2 \times 2 \times 2$ supercells starting from both the perfect lattice structure and randomized positions. All these calculations yielded one symmetrically distinct configuration. The forces for this optimal LDA + U configuration were then calculated using the HSE06 functional, which gave a maximum force that was less than 0.2 eV/Å. Further relaxation using the HSE06 functional changed the energy by less than 0.01 eV and positions by less than 0.03 Å. This demonstrates that in terms of geometries the LDA + U parametrization works remarkably well.

The STH configuration obtained in this way is shown in Fig. 2(a). STH formation leads to the emergence of a localized

[3]Note that antiferroelectric distortions, i.e., rotations of oxygen octahedra, are suppressed in the $3 \times 3 \times 3$ supercells employed in the present study.

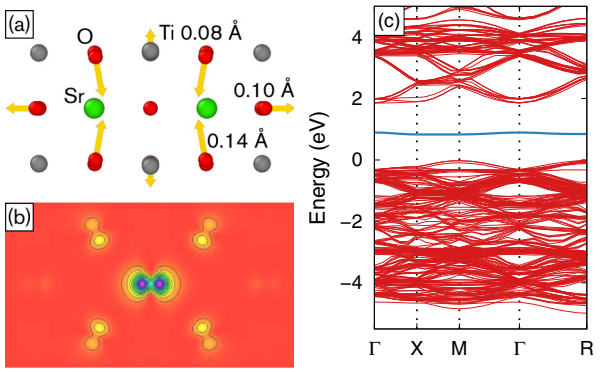

FIG. 2. (Color online) (a) Geometric structure of STH in cubic $SrTiO_3$ and (b) hole density corresponding to STH level projected onto (100) plane. (c) Band structure for $3 \times 3 \times 3$ supercell showing the STH level in the band gap (LDA + U). $\boldsymbol{k}$-point labels are equivalent to the primitive cell.

level that, as shown in Figs. 2(b) and 2(c), is located at a single oxygen site and exhibits O $2p$ character. While the oxygen atom at the center of the STH configuration remains at its ideal lattice site, the two nearest Ti neighbors are displaced outward by 0.09 Å along ⟨100⟩ and the four next-nearest O neighbors move inward by 0.12 Å along ⟨110⟩. Note that overall the ionic relaxations are small, whereas the hole has been completely localized. This is rather different from most V_K centers in halides, which typically exhibit lattice distortions on the order of 0.5 Å and above [17]. As a result the migration of the STH involves small changes in the ion positions when the localized charge is transferred between nearest-neighbor oxygen sites. This in turn implies that the nonadiabatic, in particular diabatic [33], potential-energy landscapes must be calculated in order to obtain correct rates of diffusion of these species.

C. Piecewise linearity

Thanks to the emergence of a localized level we now have a system for which we can explicitly study the variation of the total energy with fractional occupation as the localized level is gradually being filled. This is accomplished by varying the total charge in the system. Figure 3 shows that the HSE06 functional actually performs very well in producing a piecewise linear variation of the energy between integer occupations. At the same time, HSE06 predicts a band gap of 3.1 eV, in good agreement with the experimental value of 3.25 eV [34] (compare Table I). This demonstrates that in the present case HSE06 *simultaneously* provides a good description of the ideal and the self-trapped structures, supporting the suitability of this hybrid functional for the present purpose. Next we consider the variation of the total energy with fractional occupation for a series of LDA + U functionals with varying U. With increasing U the behavior changes from concave to convex as anticipated in Sec. II.[4] The best agreement is obtained for a U parameter of 7 eV, which is close to the value of 8 eV obtained by matching the forces and demonstrates the consistency of our approach. For simplicity in the following, however, we continue using a value of 8 eV. The effect of this choice on the results is small.[5]

D. STH formation energies

Formally the STH formation energy can be computed from the expression

$$\Delta\widetilde{E}_f = E^{+1}_{\mathrm{STH}} - E^{+1}_{id}, \tag{4}$$

where E^{+1}_{STH} is the total energy of the STH configuration, while E^{+1}_{id} denotes the total energy of the corresponding ideal cell.

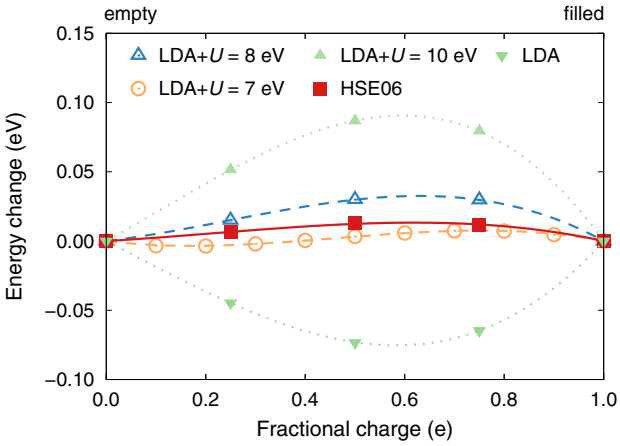

FIG. 3. (Color online) Variation in total energy with excess charge calculated using the HSE06 hybrid functional as well as several LDA + U models. Ionic positions are fixed at the relaxed STH configuration. Both HSE06 and $U = 7$ eV exhibit only small deviations from linear dependence.

Both configurations contain the same number of atoms and electrons and accordingly are in the same charge state as indicated by the superscript. Formation energies obtained from Eq. (4) are shown as filled circles (dashed lines) in Fig. 4 for different $\boldsymbol{k}$-point grids. These data illustrate that $\Delta\widetilde{E}_f$ converges rather slowly with the number of $\boldsymbol{k}$ points. This behavior is due to partially occupied states near the VBM in the charged ideal cell, which implies that convergence of the E^{+1}_{id} term in Eq. (4) requires fine $\boldsymbol{k}$-point grids (similar to metallic systems). Note that such dense sampling of the Brillouin zone is computationally prohibitively expensive for calculations involving hybrid XC functionals.

For the latter reason and to establish the connection to defect thermodynamics it is instructive to consider the following alternative relation for the formation energy:[6]

$$\Delta E_f = E^{+1}_{\mathrm{STH}} - E^{0}_{id} + q\varepsilon_{\mathrm{VBM}}, \tag{5}$$

which is of the form that is widely employed in calculations of defect formation energies; see, e.g., Refs. [37–40]. Here E^{0}_{id} is the total energy of the neutral ideal configuration, q denotes the excess charge of the defect supercell ($q = +1$ for a STH), and $\varepsilon_{\mathrm{VBM}}$ is the VBM in the perfect crystal. The valence band maximum $\varepsilon_{\mathrm{VBM}}$ (or ionization potential) is given by the total energy difference $E^{0}_{id} - E^{q}_{id}$ in the limit of vanishing excess charge density q/V, where V indicates the system volume (see, e.g., Refs. [39,40]), i.e.,

$$\varepsilon_{\mathrm{VBM}} = \lim_{V\to\infty}\left[E^{0}_{id} - E^{q}_{id}\right]/q. \tag{6}$$

This shows that in the limit of an infinitely large cell $\Delta E_f = \Delta\widetilde{E}_f$. Equation (5) has the advantage that both total energy terms, E^{+1}_{STH} and E^{0}_{id}, refer to systems that have only fully occupied or fully empty states, whence they converge rapidly

[4]One should note that image charge interactions also lead to quadratic term in fractional occupation. The very large dielectric constants of the oxides considered in this study, however, imply that in the present cases this effect is negligibly small. This is also confirmed by test calculations using larger supercells. Note that a self-consistent determination of the U parameter following for example the procedure outlined in Refs. [19,25] avoids this ambiguity and is therefore suitable for arbitrary oxides.

[5]Note that a similar value was used in a study of TiO_2 [35].

[6]In general the formation energy expression also contains terms that account for changes in the number of atoms, which is, however, of no concern here.

TABLE I. Compilation of properties computed for $SrTiO_3$, $PbTiO_3$, and $BaTiO_3$ using different approximations to the XC functional. In the case of the LDA + U functional a U parameter of 8 eV was applied exclusively to the O $2p$ states. All STH calculations were carried out at the respective equilibrium lattice parameters using $3 \times 3 \times 3$ supercells (135 atoms) and $2 \times 2 \times 2$ Monkhorst-Pack k-point grids with the exception of the calculation of the position of the STH level, which was carried out using $5 \times 5 \times 5$ Γ-centered grids.

Method	$SrTiO_3$	$PbTiO_3$	$BaTiO_3$
Lattice constant (Å)			
LDA	3.871	3.888	3.957
LDA + U	3.850	3.868	3.938
HSE06	3.908	3.923	3.993
Band gap (eV)			
LDA	1.70	1.41	1.61
LDA + U	1.85	1.37	1.78
HSE06	3.09	2.54	2.94
Experiment (Refs. [34,36])[a]	3.25	(3.2)	(3.2)
Formation energy ΔE_f according to Eq. (5) (eV)			
LDA + U	−0.09	+0.24	−0.20
HSE06	−0.09	+0.32	−0.25
STH level relative to VBM [compare Fig. 2(c)] (eV)			
LDA + U	0.88	0.56	0.87
Valence band offset relative to $BaTiO_3$ [compare Fig. 5(a)] (eV)			
LDA	0.2	0.8	
LDA + U	0.1	0.9	
HSE06	0.1	0.9	
Experiment (Ref. [36])	0.0	1.2	

[a]The experimental data are room temperature values corresponding in the case of $BaTiO_3$ and $PbTiO_3$ to the tetragonal phase.

with $\boldsymbol{k}$-point density. This is illustrated by the data shown as open squares (dotted lines) in Fig. 4.

Unfortunately, Eq. (5) involves the difference between two system with different total charges, which requires additional considerations [39–41].[7] The total energy per unit cell of an infinite system subject to periodic boundary conditions is only known to within a constant due to the exact cancellation of three infinities: the electron-electron, the ion-ion, and the electron-ion electrostatic energies [42]. The value of this constant can shift when the overall electronic charge state of each supercell in a periodic system is changed, while the total energy per unit cell is kept finite by adding a compensating homogeneous background charge [42]. To correct this shortcoming one typically applies a so-called potential alignment (PA) correction, which adds a term $q\Delta v_{\mathrm{PA}}$ to Eq. (5). The correction Δv_{PA} can be obtained by considering the shift in the electrostatic potential between the STH cell and the neutral ideal cell at a position that is "far away" from the defect [40,41]. In practice this can be accomplished by taking averages of the potential over, for example, transversal planes or over atomic core regions with very similar results; see Fig. 2 in Ref. [41]. In the present work we have adopted the latter approach and employed the average electrostatic potential shift at the atomic site that is farthest from the STH center. While as shown in Fig. 4(b) there is a large potential offset at the oxygen site at which the STH is localized, the potential shift quickly converges to a constant value as the distance to the STH increases. This is due to strong dielectric screening and demonstrates that the supercell size employed here is well suited for the present purpose. The formation energies obtained from Eq. (5) with PA corrections included are shown by filled squares (solid lines) in Fig. 4 and almost

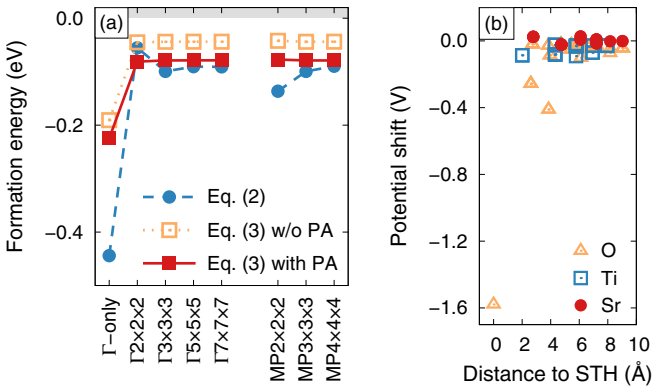

FIG. 4. (Color online) (a) Convergence of formation energy of STH in $SrTiO_3$ computed via Eqs. (5) and (4) with $\boldsymbol{k}$-point grid (LDA + U with $U(\mathrm{O}2p) = 8\,\mathrm{eV}$). The difference between the open and closed squares illustrates the effect of the potential alignment correction term $q\Delta v_{\mathrm{PA}}$. (b) Electrostatic potential shift averaged around ionic cores between neutral ideal and charged STH supercells as a function of the distance to the oxygen ion at which the STH is centered.

[7]When computing formation energies of charged defects one also must account for image charge interactions corresponding to the spurious binding between an array of localized charges and a homogeneous background [40,41,44,45]. In the present case strong dielectric screening renders this interaction, however, exceedingly small. A very conservative estimate based on the monopole-monopole interaction, which provides an upper bound for this contribution, yields a value of 7 meV, which due to its smallness has not been considered further.

coincide with the converged values obtained from Eq. (4). This comparison asserts the approximate (due to finite systems size) equivalence of the two approaches for calculating formation energies.

We are now in a position to compare formation energies obtained using the HSE06 hybrid functional with the LDA + U [$U(\mathrm{O}2p) = 8\,\mathrm{eV}$] approach. For a $2 \times 2 \times 2$ Monkhorst-Pack mesh LDA + U yields $\Delta E_f = -0.09\,\mathrm{eV}$ and $\Delta \widetilde{E}_f = -0.14\,\mathrm{eV}$, in good agreement with the values of $\Delta E_f = -0.09\,\mathrm{eV}$ and $\Delta \widetilde{E}_f = -0.16\,\mathrm{eV}$ obtained using the HSE06 hybrid functional, where the latter calculations required more than two orders of magnitude more computer time. In a previous study based on a model Hamiltonian approach parametrized using primarily experimental data, Qiu *et al.* obtained an energy gain of −0.2 eV upon STH formation, which is in reasonable agreement with the present data [11,12].

E. Extension to $BaTiO_3$ and $PbTiO_3$

In addition to $SrTiO_3$ we have considered two other cubic perovskitic titanates, namely $BaTiO_3$ and $PbTiO_3$. For $BaTiO_3$ our calculations predict STH formation with a formation energy of $\Delta E_f = -0.20\,\mathrm{eV}$ at the LDA + U level (with $U = 8\,\mathrm{eV}$ applied to O $2p$ states as in the case of $SrTiO_3$ discussed above) and $-0.25\,\mathrm{eV}$ at the HSE06 level (compare Table I). In the case of $PbTiO_3$ we obtain formation energies of $\Delta E_f = +0.24\,\mathrm{eV}$ and $+0.32\,\mathrm{eV}$ from LDA + U and HSE06 calculations, respectively. Note that the good agreement between LDA + U and HSE06 was obtained by simply using the same U parameter as in the case of $SrTiO_3$, which suggests that the parameter is reasonably transferable at least within this group of rather similar oxides.

The relaxation patterns for $SrTiO_3$ and $BaTiO_3$ are rather similar. For $PbTiO_3$ one observes that while the displacements in the vicinity of the STH are similar to $SrTiO_3$ and $BaTiO_3$ the relaxation pattern is more long ranged, i.e., also ions that are farther from the STH center exhibit noticeable displacements. This behavior is related to the strong coupling between Pb 6s states and O $2p$ that is discussed below.

It is instructive to compare our results with previous studies. Embedded cluster calculations based on the HF approximation yielded "hole trapping energies," which should be comparable to the formation energies obtained in the present study, of $-1.49\,\mathrm{eV}$ for cubic $BaTiO_3$ [9] and $-0.87\,\mathrm{eV}$ for tetragonal $BaTiO_3$ [10]. Given the tendency of the HF method to overestimate localization as discussed in Sec. II it is not surprising that these values are much more negative than the ones obtained in the present work. They are also associated with band gaps of 5.4 and 6.1 eV for cubic and tetragonal $BaTiO_3$, respectively, that are considerably larger than the experimental values (see Table I). In agreement with the present study, the relaxation pattern obtained in these studies includes an outward relaxation of the two nearest Ti neighbors and an inward relaxation of the next nearest O neighbors by about 0.1 Å.

The positive STH formation energy in the case of $PbTiO_3$ implies that localized holes are metastable and energetically less favorable than their delocalized (band) counterparts and thus should not occur under normal conditions. This begs the question of what distinguishes $PbTiO_3$ from $BaTiO_3$ and $SrTiO_3$ when it comes to STH formation. The situation can be rationalized by considering the position of the VBM in the different materials.[8] Figure 5(a) shows the shift in the VBM for $PbTiO_3$ and $SrTiO_3$ with respect to $BaTiO_3$, which reveals that with respect to an absolute energy scale the VBM in $PbTiO_3$ is markedly higher than in either $BaTiO_3$ or $SrTiO_3$. The energy scales were aligned using the electrostatic potentials averaged around the oxygen cores (obtained in the same way as for the PA correction; see Sec. III D). Alternatively one can also employ the O 1s core levels for alignment, which, as demonstrated by the last data set in Fig. 5(a), leads to very similar results.[9] This approach was employed previously to determine the VBM offset between the rutile and anatase phases of titania [43]. Also the offsets thus obtained are in good agreement with recent experimental data [36], which gives VBM offsets of 1.2 ± 0.1 eV and 0.0 ± 0.1 eV for $PbTiO_3$ and $SrTiO_3$ relative to $BaTiO_3$, respectively (also compare Table I).

Figures 2(b) and 2(c) show that STH formation leads to the emergence of a localized atomlike level above the VBM. In the case of $PbTiO_3$ this O level is noticeably closer to the VBM (see Table I). This suggests that STH formation is energetically less favorable and provides a rationale for the positive STH formation energy in $PbTiO_3$.

It still remains to explore the origin of the higher lying VBM in $PbTiO_3$ compared to $BaTiO_3$ and $SrTiO_3$. To this end, we show in Figs. 5(b)–5(d) the band structures of the three materials in question. While the valence band edges of $SrTiO_3$ and $BaTiO_3$ are similar in the case of $PbTiO_3$ one observes a distinct band splitting around the X point, which forms the VBM and gives rise to a tail in the density of states; compare Fig. 5(e). The feature is caused by the interaction of Pb 6s states, which are spatially rather extended and energetically located just beneath the topmost valence band [see Fig. 5(c)], with O $2p$ states, which constitute the top of the valence band. Strong s-p coupling and large upward VBM shifts are also observed, for example, in Bi compounds [36] for similar reasons. This coupling is also responsible for the more extended relaxation pattern around a STH in $PbTiO_3$ compared to $SrTiO_3$ and $BaTiO_3$ that was alluded to above.

Based on this argument one can thus expect that within this group of materials VBM alignment can serve as a good predictor for STH formation (or absence thereof) insofar as it is reflective of the coupling of low-lying cation states to the O$2p$ states comprising the valence band. One can furthermore anticipate that increasing the lattice constant should lead to stronger self-trapping and thus more negative formation energies since it allows for more ionic relaxation. This is indeed observed as shown in Fig. 6(a), which shows the STH formation energies for the three compounds considered in this study as a function of lattice parameter. For $BaTiO_3$ and $SrTiO_3$ one obtains similar formation energies and a modest decrease of ΔE_f with lattice expansion.

[8]Note that a similar form of alignment was observed in the case of rutile and anatase TiO_2; see Ref. [46].

[9]The O 1s core levels were obtained by evaluating the Kohn-Sham energies for the core states based on the self-consistently determined valence charge density (initial state approximation); Ref. [47].

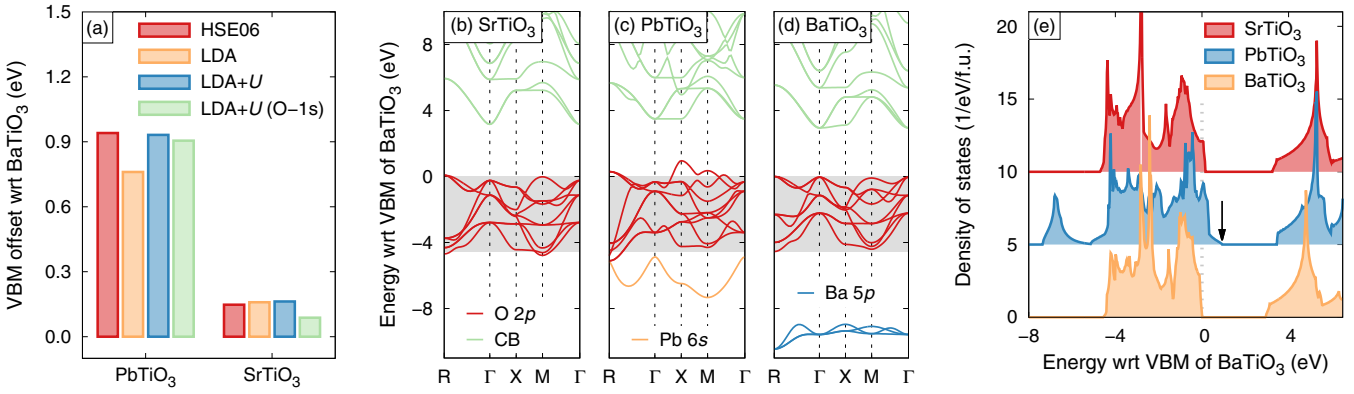

FIG. 5. (Color online) (a) Band lineup for $BaTiO_3$, $PbTiO_3$, and $SrTiO_3$ according to different XC functionals. [(b)–(d)] Band structures and (e) densities of states for $SrTiO_3$, $PbTiO_3$, and $BaTiO_3$ according to LDA + U calculations with scissor corrections. The significantly higher VBM in $PbTiO_3$ originates from the coupling between O $2p$ and Pb $6s$ states. The latter appear just below the O $2p$ derived topmost valence band and are visible in both panels (c) and (e) between approximately -4 and -8 eV. The bands in panels (b)–(d) have been colored according to the dominant character of the entire band manifold to indicate the assignments qualitatively rather than quantitatively. The arrow in panel (e) indicates the position of the VBM in $PbTiO_3$.

By contrast, $PbTiO_3$ exhibits a much stronger variation of the formation energy with volume. First we note that the lattice expansion has a negligible effect on the "bump" at the VBM that is apparent in Fig. 5(d) and caused by the coupling between O $2p$ and Pb $6s$ states. The strong coupling rather manifests itself in a more pronounced contribution of Pb ions to the STH relaxation than the A-site ions in $SrTiO_3$ and $BaTiO_3$; see Figs. 6(b) and 6(c). These effects are enhanced as the lattice constant increases and cause a substantial nonlinear drop of the formation energy with increasing lattice constant. This actually suggests that STH formation at the (charge) densities corresponding to the supercell sizes considered here ($3 \times 3 \times 3$) can destabilize the crystal structure.

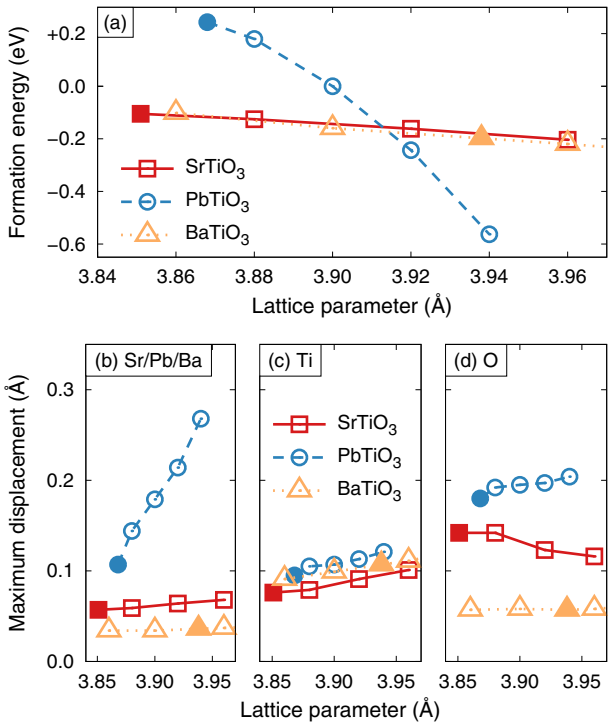

FIG. 6. (Color online) (a) STH formation energies and (b)–(d) maximum atomic displacements per atom type for cubic $SrTiO_3$, $PbTiO_3$, and $BaTiO_3$ as a function of lattice parameter. Filled symbols indicate data corresponding to the equilibrium lattice constant.

IV. CONCLUSIONS

In summary we have demonstrated from a methodological standpoint that (i) the application of LDA + U potentials to O $2p$ states can be physically motivated in the case of self-trapping in oxides, (ii) suitable parametrizations match the forces and energetics of hybrid functionals well, and (iii) both LDA + U parametrizations and the HSE06 functional are reasonably close to piecewise linearity in the case of STHs in the perovskite oxides considered in this study. In terms of materials, relevant results show that hole self-trapping should occur in $SrTiO_3$ and $BaTiO_3$ but not $PbTiO_3$. The absence of bulk STHs in the latter case can be explained by the higher VBM compared to the other two materials, which originates from strong coupling between Pb $6s$ and O $2p$ states. The results described in this paper provide a basis for similar studies in other oxide materials. They illustrate what kind of effects should be taken into account and indicate which fundamental parameters can serve as approximate predictors for the presence or absence of self trapping.

In closing we point out that in general the correction (i.e., the U parameter(s) in DFT + U or the parameters of the hybrid XC functional) that yields piecewise linear behavior is state and configuration dependent. In the present case this turned out not be an issue as the dependence of U on the configuration was found to be small and furthermore the HSE06 functional gave both piecewise linearity for the STH and good agreement with the experimental band gap.

ACKNOWLEDGMENTS

P.E. acknowledges funding from the Area of Advance–Materials Science at Chalmers, the Swedish Research Council in the form of a young researcher grant, and the European Research Council via a Marie Curie career integration grant.

A.K. acknowledges support by the German Science Foundation via the collaborative research center on electrical fatigue of functional materials (SFB 595). D.Å. and B.S. acknowledge funding from the NA-22 agency. Parts of this work were prepared at Lawrence Livermore National Laboratory, which is operated by Lawrence Livermore National Security, LLC, for the U.S. DOE-NNSA under Contract No. DE-AC52-07NA27344. Computer time allocations by the Swedish National Infrastructure for Computing at NSC (Linköping) and C3SE (Gothenburg) are gratefully acknowledged.

[1] O. F. Schirmer, J. Phys.: Condens. Matter **18**, R667 (2006).
[2] A. M. Stoneham, J. L. Gavartin, A. Shluger, A. V. Kimmel, D. M. Ramo, H. M. Ronnow, G. Aeppli, and C. Renner, J. Phys.: Condens. Matter **19**, 255208 (2007).
[3] A. L. Shluger, K. P. McKenna, P. V. Sushko, D. Muñoz Ramo, and A. V. Kimmel, Modelling Simul. Mater. Sci. Eng. **17**, 084004 (2009).
[4] T. Holstein, Ann. Phys. **8**, 325 (1959).
[5] A. L. Shluger and A. M. Stoneham, J. Phys.: Condens. Matter **5**, 3049 (1993).
[6] H. Ihrig, J. Phys. C: Solid State Phys. **9**, 3469 (1976).
[7] J. v. d. Brink and D. I. Khomskii, J. Phys.: Condens. Matter **20**, 434217 (2008).
[8] S. Picozzi and A. Stroppa, Eur. Phys. J. B **85**, 1 (2012).
[9] A. Stashans and H. Pinto, Internat. J. Quantum Chem. **79**, 358 (2000).
[10] H. Pinto and A. Stashans, Phys. Rev. B **65**, 134304 (2002).
[11] Y. Qiu, C. Q. Wu, and K. Nasu, Phys. Rev. B **72**, 224105 (2005).
[12] Y. Qiu, Y.-J. Jiang, G.-P. Tong, and J.-F. Zhang, Phys. Lett. A **372**, 2920 (2008).
[13] C. Franchini, G. Kresse, and R. Podloucky, Phys. Rev. Lett. **102**, 256402 (2009).
[14] E. A. Kotomin, R. I. Eglitis, and G. Borstel, J. Phys.: Condens. Matter **12**, L557 (2000).
[15] V. I. Anisimov, J. Zaanen, and O. K. Andersen, Phys. Rev. B **44**, 943 (1991).
[16] J. L. Gavartin, P. V. Sushko, and A. L. Shluger, Phys. Rev. B **67**, 035108 (2003).
[17] B. Sadigh, P. Erhart, and D. Åberg, arXiv:1401.7137 .
[18] J. P. Perdew and A. Zunger, Phys. Rev. B **23**, 5048 (1981).
[19] M. Cococcioni and S. de Gironcoli, Phys. Rev. B **71**, 035105 (2005).
[20] I. Dabo, A. Ferretti, N. Poilvert, Y. Li, N. Marzari, and M. Cococcioni, Phys. Rev. B **82**, 115121 (2010).
[21] S. Lany and A. Zunger, Phys. Rev. B **80**, 085202 (2009).
[22] P. Zawadzki, J. Rossmeisl, and K. W. Jacobsen, Phys. Rev. B **84**, 121203 (2011).
[23] J. P. Perdew, A. Ruzsinszky, G. I. Csonka, O. A. Vydrov, G. E. Scuseria, V. N. Staroverov, and J. M. Tao, Phys. Rev. A **76**, 040501 (2007).
[24] P. Mori-Sanchez, A. J. Cohen, and W. T. Yang, Phys. Rev. Lett. **100**, 146401 (2008).
[25] V. I. Anisimov and O. Gunnarsson, Phys. Rev. B **43**, 7570 (1991).
[26] W. Känzig, Phys. Rev. **99**, 1890 (1955).
[27] P. H.-L. Sit, M. Cococcioni, and N. Marzari, Phys. Rev. Lett. **97**, 028303 (2006).
[28] P. E. Blöchl, Phys. Rev. B **50**, 17953 (1994); G. Kresse and D. Joubert, *ibid.* **59**, 1758 (1999).
[29] G. Kresse and J. Hafner, Phys. Rev. B **47**, 558 (1993); **49**, 14251 (1994); G. Kresse and J. Furthmüller, *ibid.* **54**, 11169 (1996); Comput. Mater. Sci. **6**, 15 (1996).
[30] S. L. Dudarev, G. A. Botton, S. Y. Savrasov, C. J. Humphreys, and A. P. Sutton, Phys. Rev. B **57**, 1505 (1998).
[31] J. Heyd, G. E. Scuseria, and M. Ernzerhof, J. Chem. Phys. **118**, 8207 (2003); **124**, 219906 (2006).
[32] J. Paier, R. Hirschl, M. Marsman, and G. Kresse, J. Chem. Phys. **122**, 234102 (2005); R. Wahl, D. Vogtenhuber, and G. Kresse, Phys. Rev. B **78**, 104116 (2008).
[33] R. A. Marcus, J. Chem. Phys. **24**, 966 (1956).
[34] K. van Benthem, C. Elsässer, and R. H. French, J. Appl. Phys. **90**, 6156 (2001).
[35] B. J. Morgan and G. W. Watson, Phys. Rev. B **80**, 233102 (2009).
[36] R. Schafranek, S. Li, F. Chen, W. Wu, and A. Klein, Phys. Rev. B **84**, 045317 (2011); S. Li, J. Morasch, A. Klein, C. Chirila, L. Pintilie, L. Jia, K. Ellmer, M. Naderer, K. Reichmann, M. Gröting, and K. Albe, *ibid.* **88**, 045428 (2013).
[37] S. B. Zhang and J. E. Northrup, Phys. Rev. Lett. **67**, 2339 (1991).
[38] D. Åberg, P. Erhart, A. J. Williamson, and V. Lordi, Phys. Rev. B **77**, 165206 (2008).
[39] C. Persson, Y.-J. Zhao, S. Lany, and A. Zunger, Phys. Rev. B **72**, 035211 (2005).
[40] S. Lany and A. Zunger, Phys. Rev. B **78**, 235104 (2008).
[41] H.-P. Komsa, T. T. Rantala, and A. Pasquarello, Phys. Rev. B **86**, 045112 (2012).
[42] J. Ihm, A. Zunger, and M. L. Cohen, J. Phys. C: Solid State Phys. **12**, 4409 (1979).
[43] G. Makov and M. C. Payne, Phys. Rev. B **51**, 4014 (1995).
[44] P. Erhart, K. Albe, and A. Klein, Phys. Rev. B **73**, 205203 (2006).
[45] P. Deák, B. Aradi, and T. Frauenheim, Phys. Rev. B **86**, 195206 (2012).
[46] L. Köhler and G. Kresse, Phys. Rev. B **70**, 165405 (2004).
[47] V. Pfeifer, P. Erhart, S. Li, K. Rachut, J. Morasch, J. Brötz, P. Reckers, T. Mayer, S. Rühle, A. Zaban, I. Mora Seró, J. Bisquert, W. Jaegermann, and A. Klein, J. Phys. Chem. Lett. **4**, 4182 (2013); S. Li, F. Chen, R. Schafranek, T. Bayer, K. Rachut, A. Fuchs, S. Siol, M. Weidner, V. Pfeifer, J. Morasch, C. Ghinea, E. Arveux, R. Günzler, J. Gassmann, C. Körber, Y. Gassenbauer, F. Säuberlich, G. V. Rao, S. Payan, M. Maglione, C. Chirila, L. Pintilie, L. Jia, K. Ellmer, M. Naderer, K. Reichmann, U. Böttger, R. Frunza, H. Uršič, B. Malič, W.-B. Wu, P. Erhart, and A. Klein, Phys. Status Solidi RRL **8**, 571 (2014).